# A Bayesian Compressive Sensing Method for Robust Diagnosis of Planar Arrays from Far-Field Measurements

M. Salucci, A. Gelmini, G. Oliveri, and A. Massa

**Abstract**

In this work, the diagnosis of planar phased antenna arrays from far-field measurements is addressed. The inverse problem at hand is formulated as a sparse retrieval one devoted at reconstructing the faulty radiators within the antenna under test. Towards this end, a Bayesian compressive sensing (*BCS*)-based method is developed to deal with the planar array diagnosis without requiring that the involved measurement operator a-priori satisfies the restricted isometry property (*RIP*). Furthermore, the proposed diagnosis tool is able to take into account the presence of real radiators, as well as to consider mutual coupling effects arising in realistic operative conditions. Some representative numerical examples are presented in order to verify the effectiveness of the proposed diagnosis tool.

# Contents

# 1 Numerical Validation

## 1.1 Uniform Array, $N = 81$, Dipole Radiators

### Parameters

- Gold Array
  - Total number of elements: $N = 81$;
  - Type of elements: $y$-oriented quarter-wave dipoles;
  - Spacing along $x$ and $y$: $d_x = d_y = 0.5$ $[\lambda]$;
  - Excitation tapering: Uniform ($w_n = 1$, $n = 1, ..., N$);

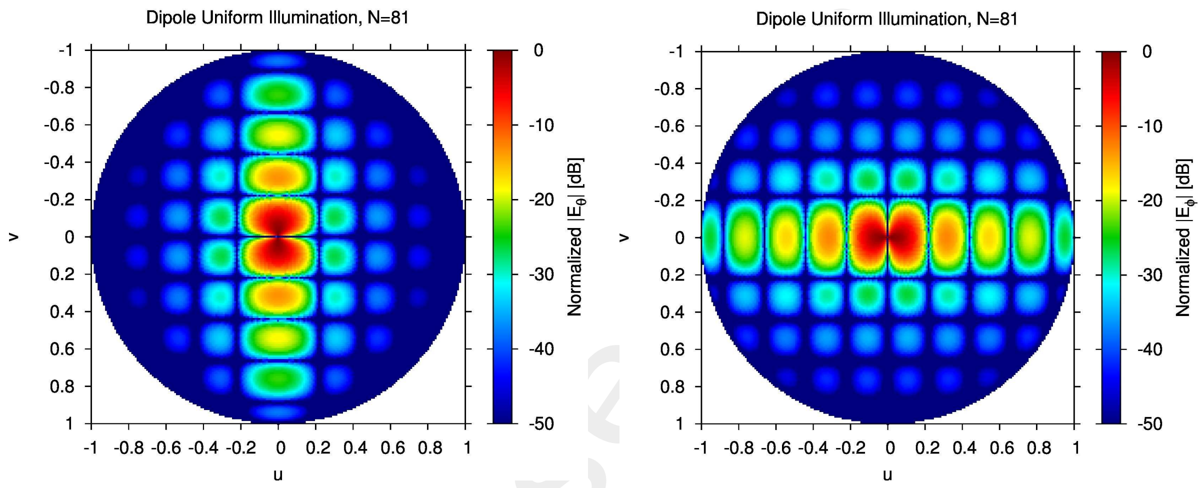


$(a)$ $(b)$

Figure 1: Normalized $(a)$ $E_\theta\,(u, v)$ and $(b)$ $E_\phi\,(u, v)$ pattern components of the gold array computed via full-wave simulation.

- Failed Array
  - Failure factor: $\kappa = 0$ (total failures);
  - Failure rate: see table below;

| $N_f$ | $\Phi = \frac{N_f}{N}$ |
|---|---|
| 1 | 1% |
| 2 | 2% |
| 3 | 4% |
| 6 | 8% |
| 13 | 16% |

Table 1: Number of failures ($N_f$) and corresponding failure rate ($\Phi = \frac{N_f}{N}$).

- Measurement set-up
  - Type of sampling: uniform sampling in the $(u, v)$ plane;

- Number of points in the visible range: $K = 81$;
- Ratio between measurements and number of elements: $\nu = \frac{K}{N} \simeq 1.0$ ($\nu^{(opt)}$);

- *BCS* solver
  - Noise variance: $\eta = 5 \times 10^{-1}$ ($\eta^{(opt)}$);
  - Tolerance factor: $\iota = 10^{-8}$;

- Signal-to-Noise-Ratio: $SNR = \{10; 20; ...; 100\}$.

### Results

**$\Phi = \frac{N_f}{N} = 1\%$ ($N_f = 1$) - Best and Worst $BCS$ Reconstructions**

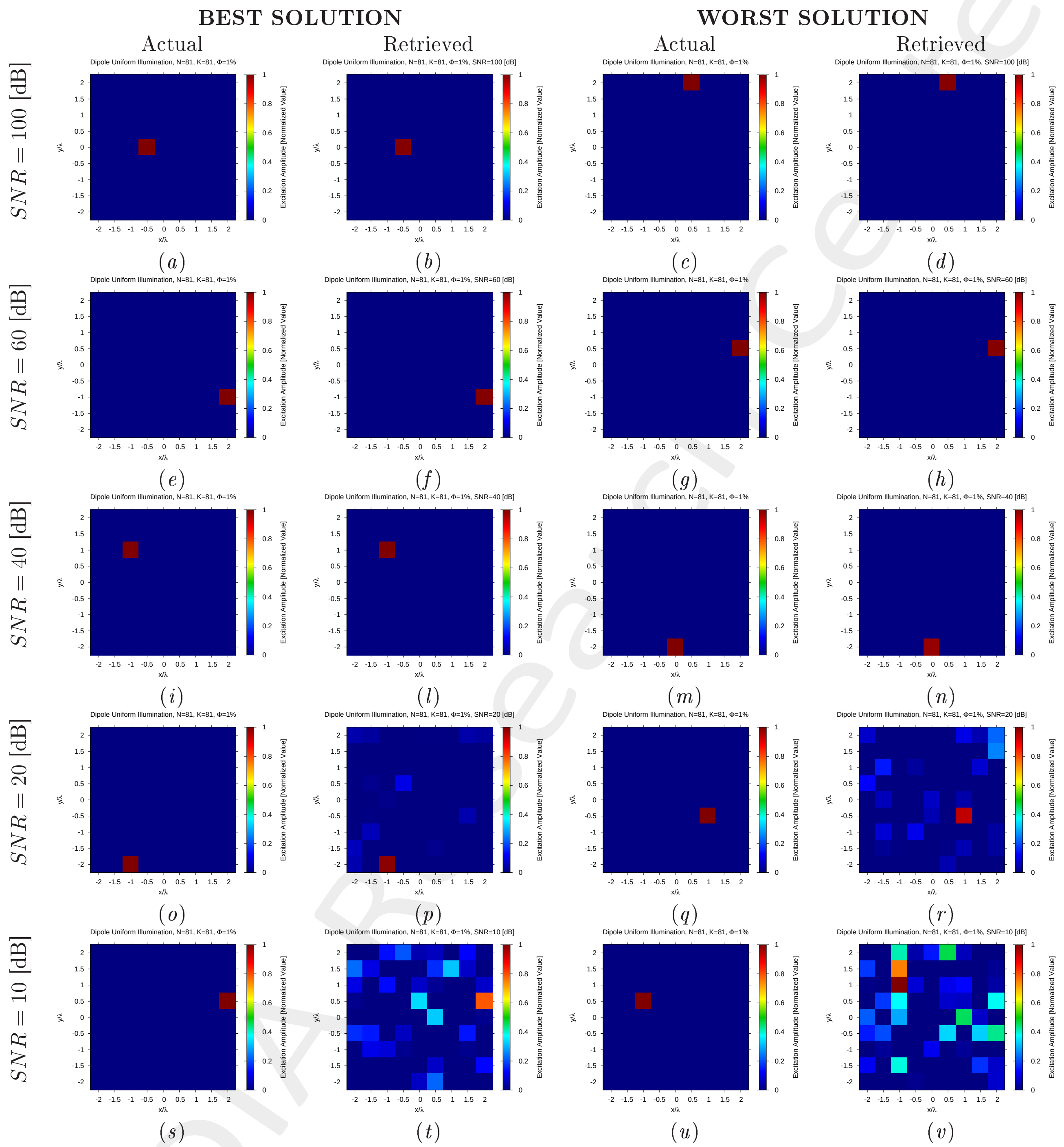


Figure 2: Uniform Dipoles Array ($N = 81$, $d_x = d_y = 0.5$ [$\lambda$],$\Phi = 1\%$) - Best and worst reconstructions by $BCS$ under several $SNR$ values.

$\Phi = \frac{N_f}{N} = 2\%$ $(N_f = 2)$ - **Best and Worst $BCS$ Reconstructions**

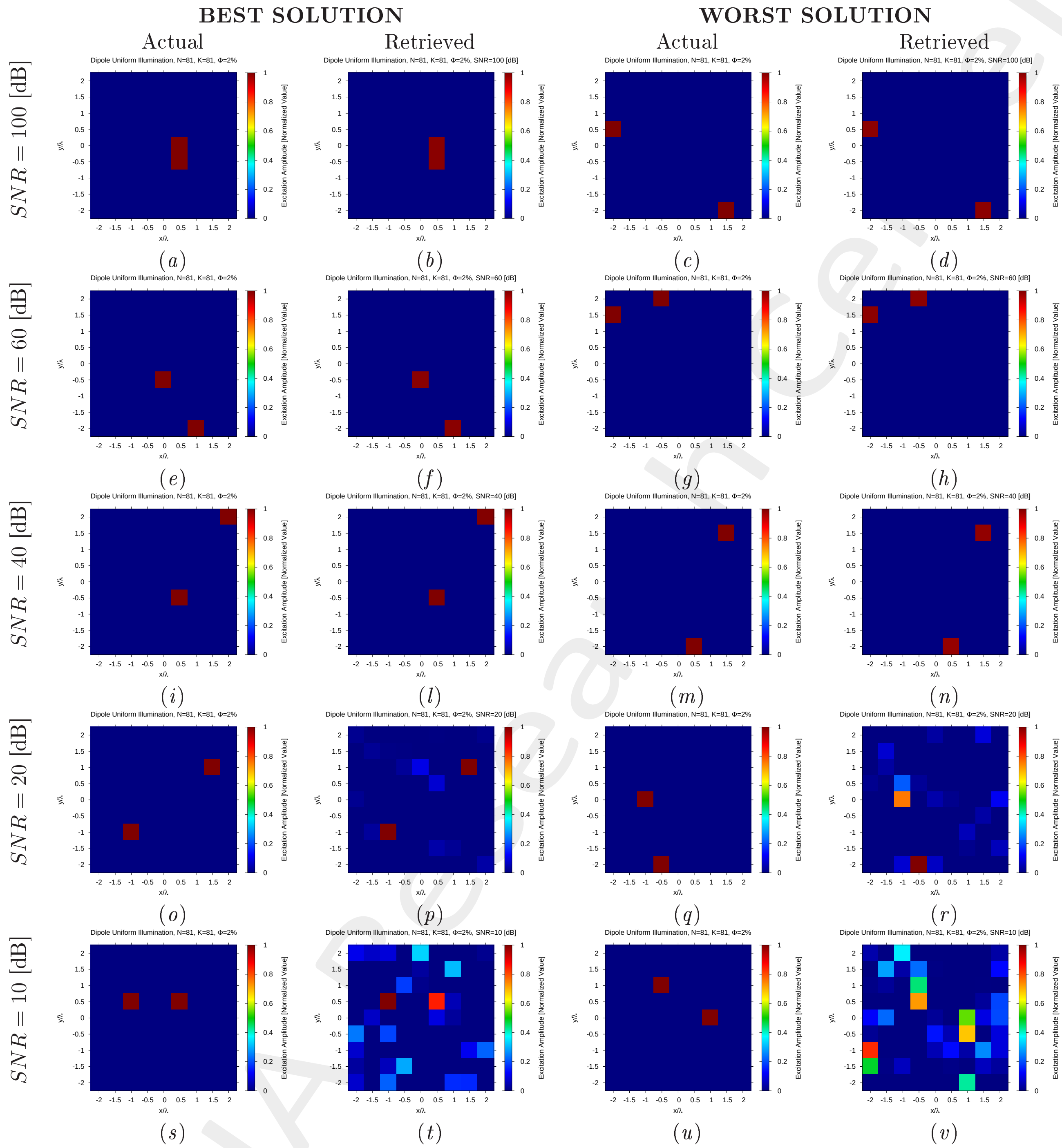


Figure 3: Uniform Dipoles Array ($N = 81$, $d_x = d_y = 0.5$ $[\lambda]$,$\Phi = 2\%$) - Best and worst reconstructions by $BCS$ under several $SNR$ values.

$\Phi = \frac{N_f}{N} = 4\%$ $(N_f = 3)$ - **Best and Worst** $BCS$ **Reconstructions**

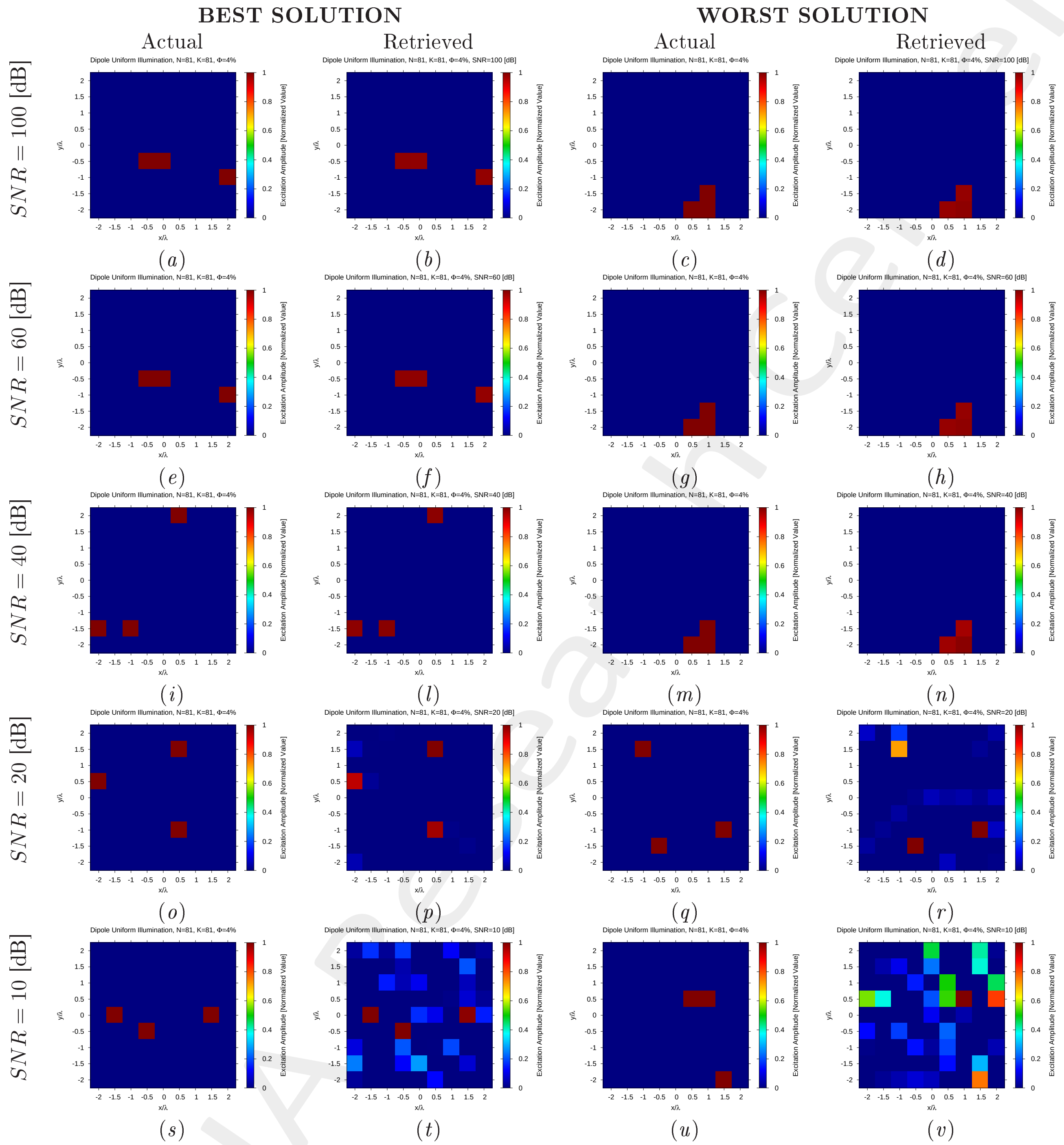


Figure 4: Uniform Dipoles Array ($N = 81$, $d_x = d_y = 0.5$ $[\lambda]$,$\Phi = 4\%$) - Best and worst reconstructions by $BCS$ under several $SNR$ values.

$\Phi = \frac{N_f}{N} = 8\%$ $(N_f = 6)$ **- Best and Worst** $BCS$ **Reconstructions**

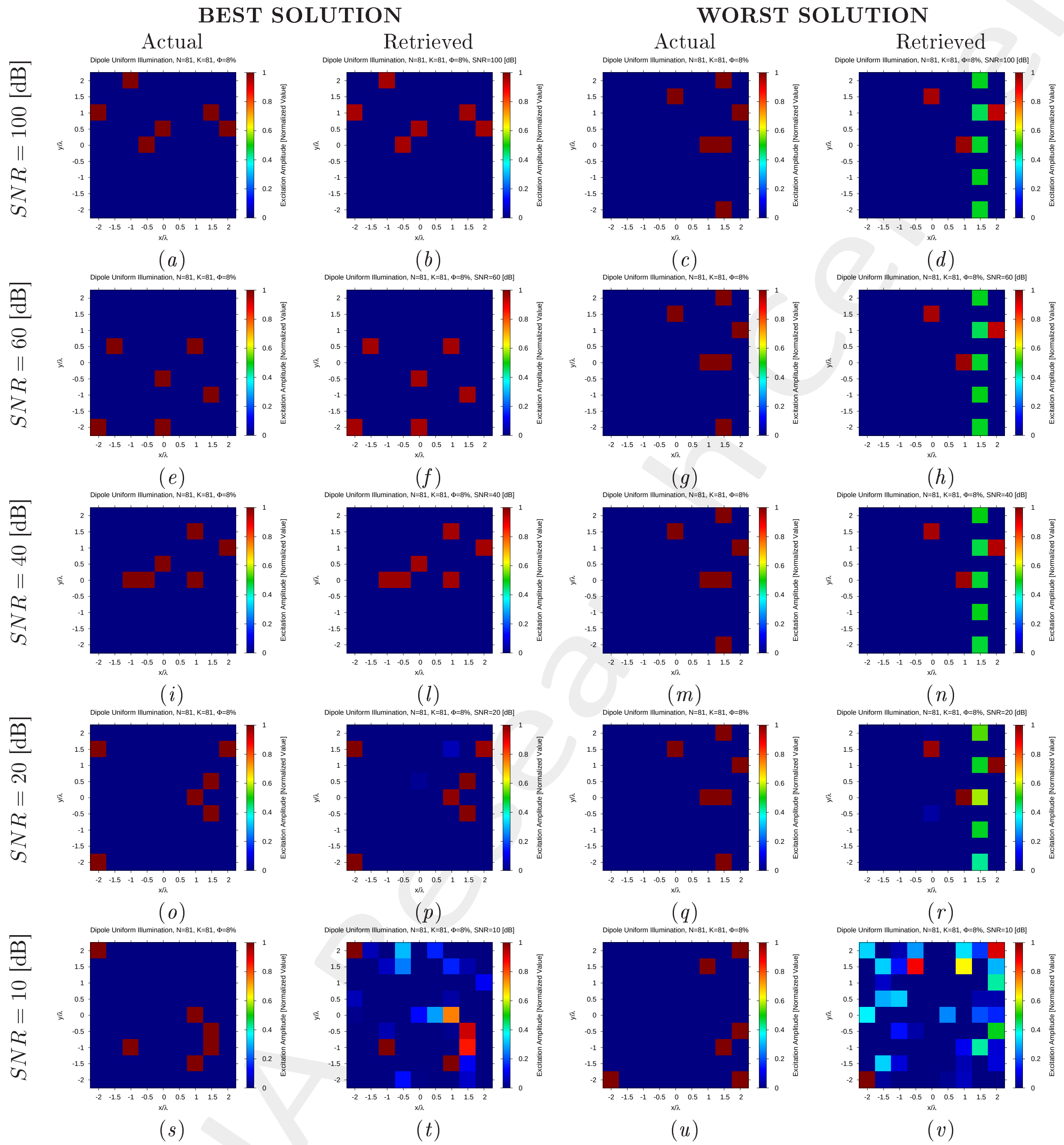


Figure 5: Uniform Dipoles Array ($N = 81$, $d_x = d_y = 0.5$ $[\lambda]$,$\Phi = 8\%$) - Best and worst reconstructions by $BCS$ under several $SNR$ values.

$\Phi = \frac{N_f}{N} = 16\%$ $(N_f = 13)$ - **Best and Worst** $BCS$ **Reconstructions**

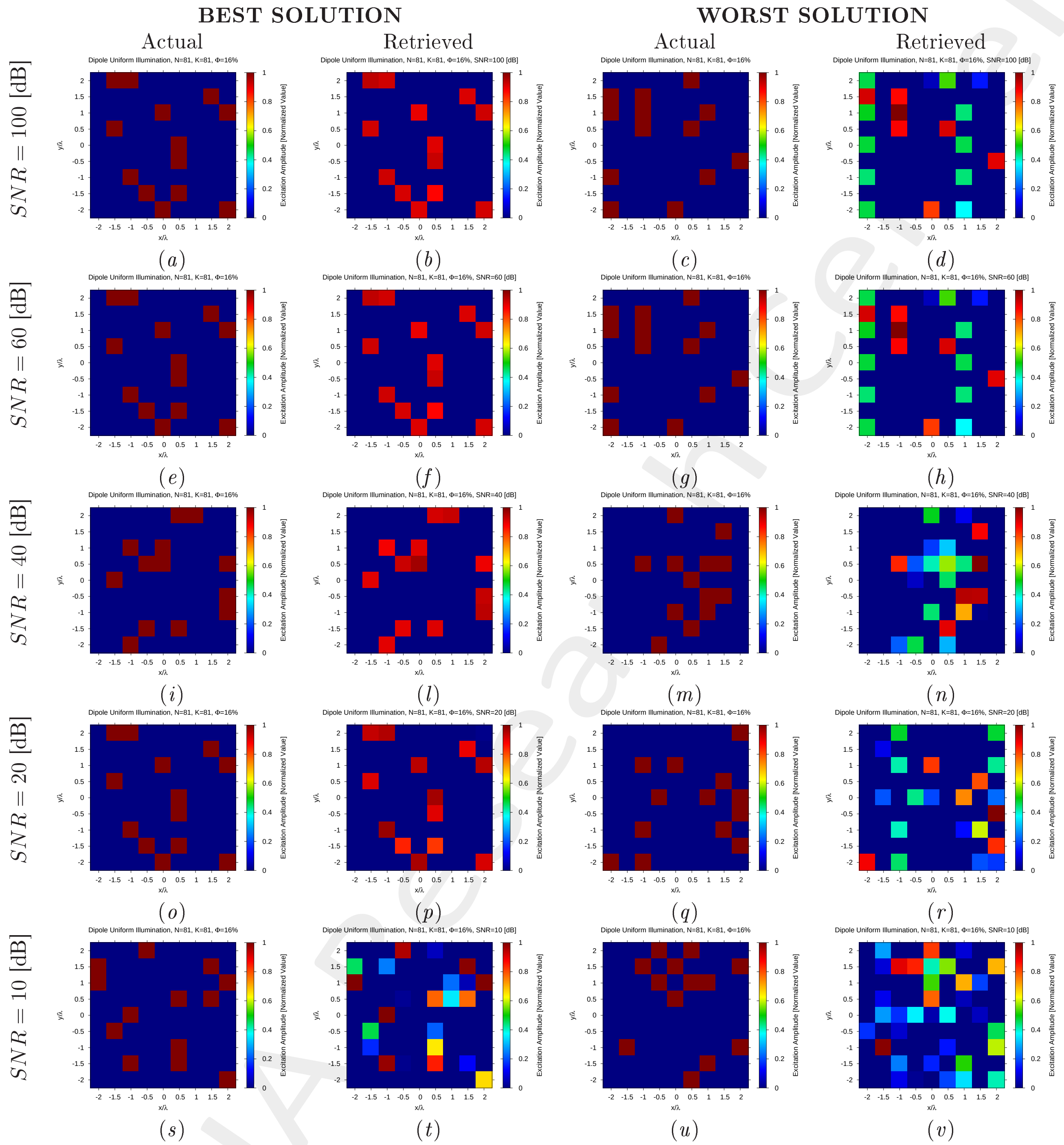


Figure 6: Uniform Dipoles Array ($N = 81$, $d_x = d_y = 0.5$ [$\lambda$],$\Phi = 16\%$) - Best and worst reconstructions by $BCS$ under several $SNR$ values.

## Diagnosis Error and Confidence Level

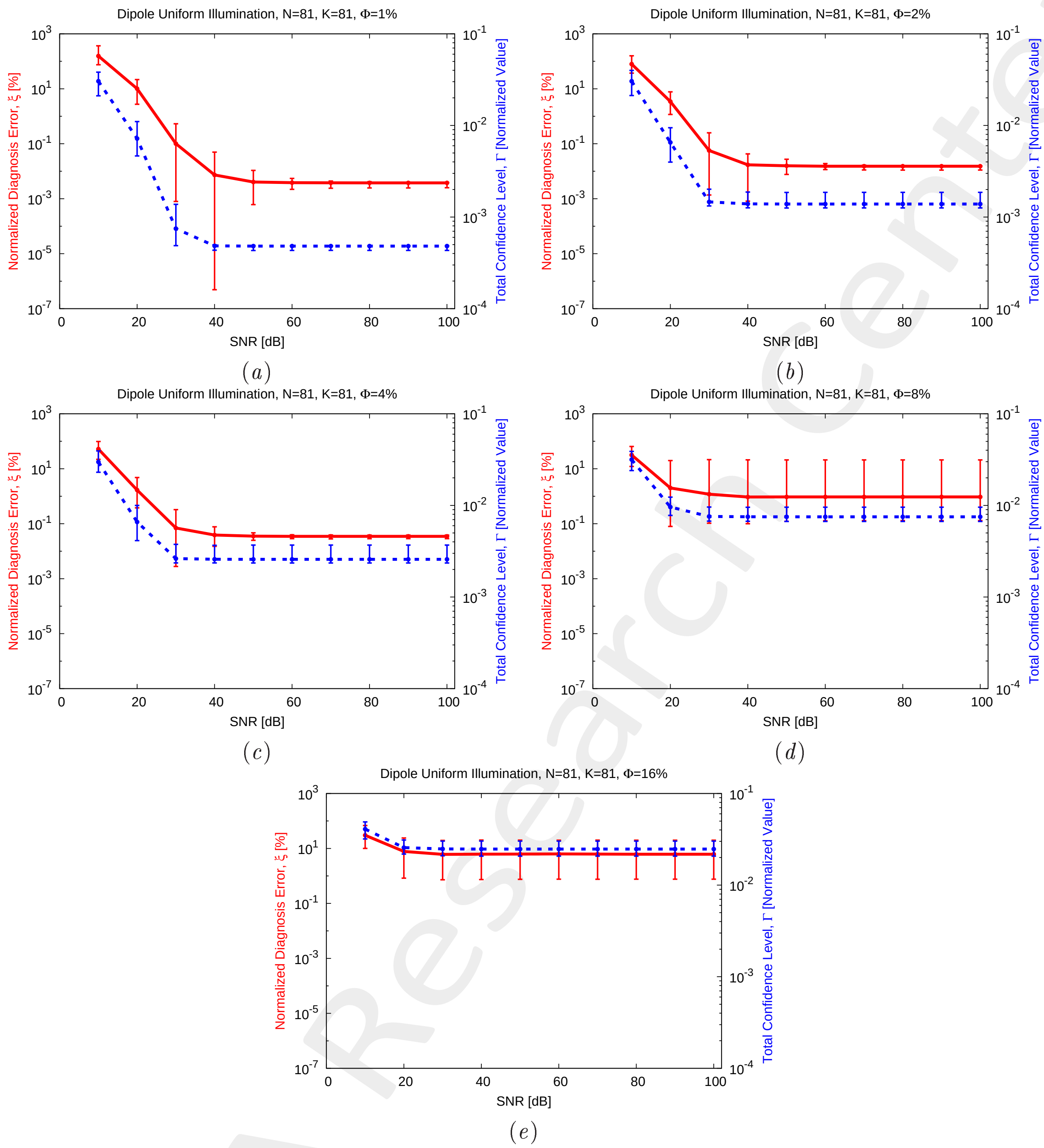


Figure 7: Uniform Dipoles Array ($N = 81$, $d_x = d_y = 0.5$ [$\lambda$]) - Behavior of the average, minimum and maximum diagnosis error ($\xi$) and total confidence level ($\Gamma$) versus the $SNR$, for ($a$) $\Phi = 1\%$, ($b$) $\Phi = 2\%$, ($c$) $\Phi = 4\%$, ($d$) $\Phi = 8\%$, and ($e$) $\Phi = 16\%$.

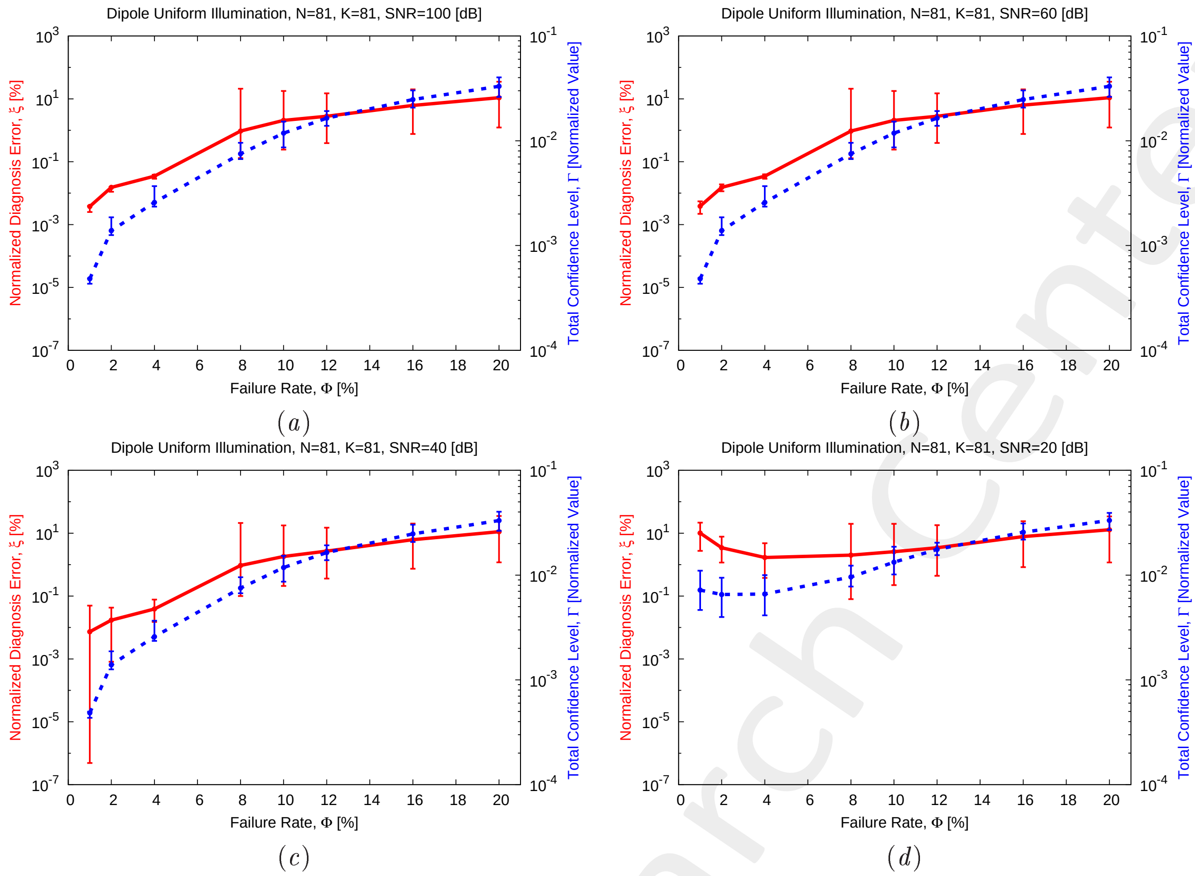


Figure 8: Uniform Dipoles Array ($N = 81$, $d_x = d_y = 0.5$ [$\lambda$]) - Behavior of the average, minimum and maximum diagnosis error ($\xi$) and total confidence level ($\Gamma$) versus the failure rate ($\Phi$), for ($a$) $SNR = 100$ [dB], ($b$) $SNR = 60$ [dB], ($c$) $SNR = 40$ [dB], and ($d$) $SNR = 20$ [dB].

## 1.2 Uniform Array, $N = 144$, Dipole Radiators

### Parameters

- Gold Array
  - Total number of elements: $N = 144$;
  - Type of elements: $y$-oriented quarter-wave dipoles;
  - Spacing along $x$ and $y$: $d_x = d_y = 0.5$ $[\lambda]$;
  - Excitation tapering: Uniform ($w_n = 1$, $n = 1, ..., N$);

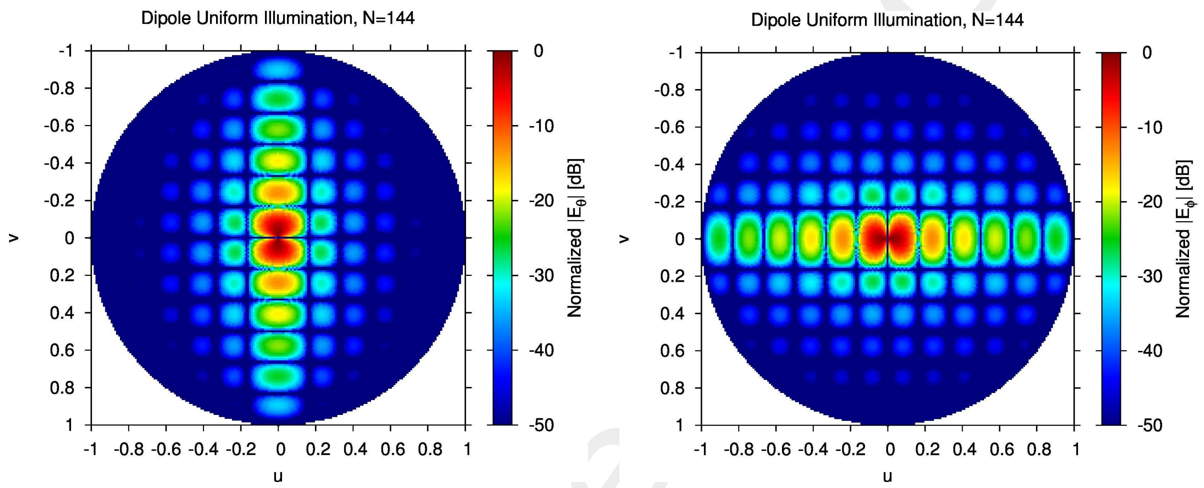


$(a)$ $(b)$

Figure 9: Normalized $(a)$ $E_\theta\,(u, v)$ and $(b)$ $E_\phi\,(u, v)$ pattern components of the gold array computed via full-wave simulation.

- Failed Array
  - Failure factor: $\kappa = 0$ (total failures);
  - Failure rate: see table below;

| $N_f$ | $\Phi = \frac{N_f}{N}$ |
|---|---|
| 1 | 1% |
| 3 | 2% |
| 6 | 4% |
| 12 | 8% |
| 23 | 16% |

Table 2: Number of failures ($N_f$) and corresponding failure rate ($\Phi = \frac{N_f}{N}$).

- Measurement set-up
  - Type of sampling: uniform sampling in the $(u,\, v)$ plane;
  - Number of points in the visible range: $K = 149$;

  - Ratio between measurements and number of elements: $\nu = \frac{K}{N} \simeq 1.0$ ($\nu^{(opt)}$);

- $BCS$ solver

  - Noise variance: $\eta = 5 \times 10^{-1}$ ($\eta^{(opt)}$);

  - Tolerance factor: $\iota = 10^{-8}$;

- Signal-to-Noise-Ratio: $SNR = \{10; 20; ...; 100\}$.

### Results

**$\Phi = \frac{N_f}{N} = 1\%$ ($N_f = 1$) - Best and Worst $BCS$ Reconstructions**

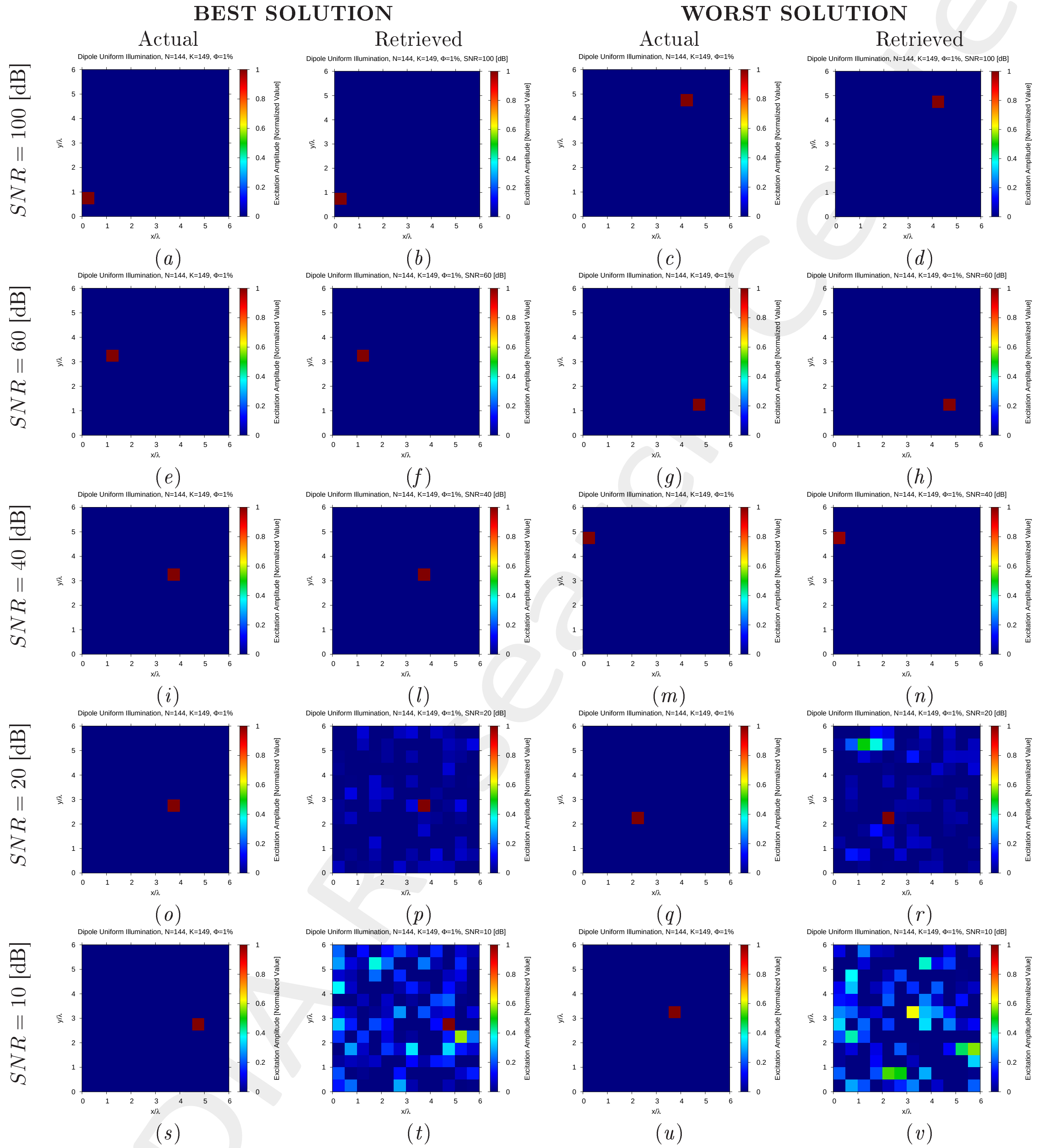


Figure 10: Uniform Dipoles Array ($N = 144$, $d_x = d_y = 0.5$ [$\lambda$], $\Phi = 1\%$) - Best and worst reconstructions by $BCS$ under several $SNR$ values.

$\Phi = \frac{N_f}{N} = 2\%$ $(N_f = 3)$ - **Best and Worst** $BCS$ **Reconstructions**

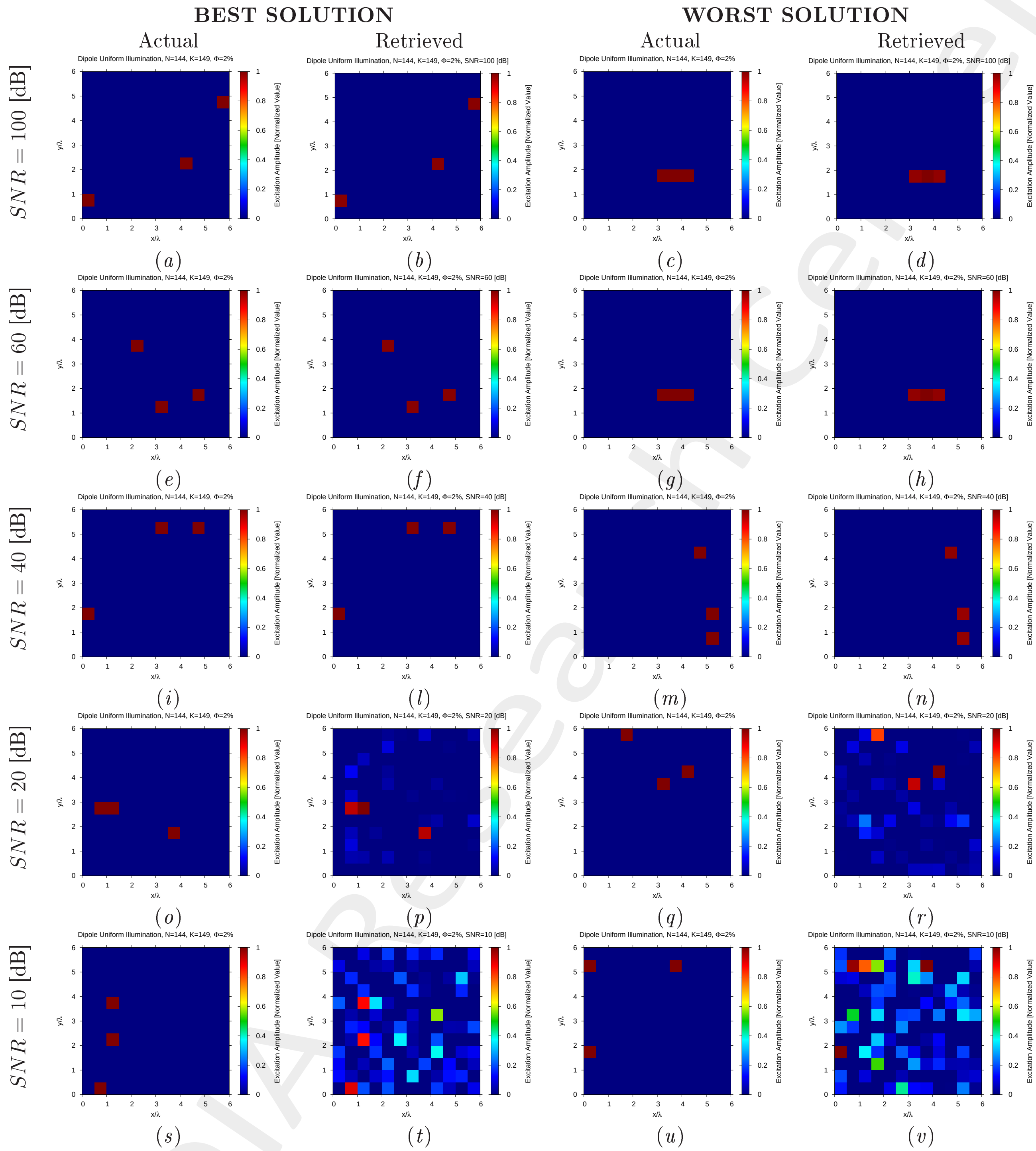


Figure 11: Uniform Dipoles Array ($N = 144$, $d_x = d_y = 0.5$ [$\lambda$], $\Phi = 2\%$) - Best and worst reconstructions by $BCS$ under several $SNR$ values.

$\Phi = \frac{N_f}{N} = 4\%$ $(N_f = 6)$ - **Best and Worst** $BCS$ **Reconstructions**

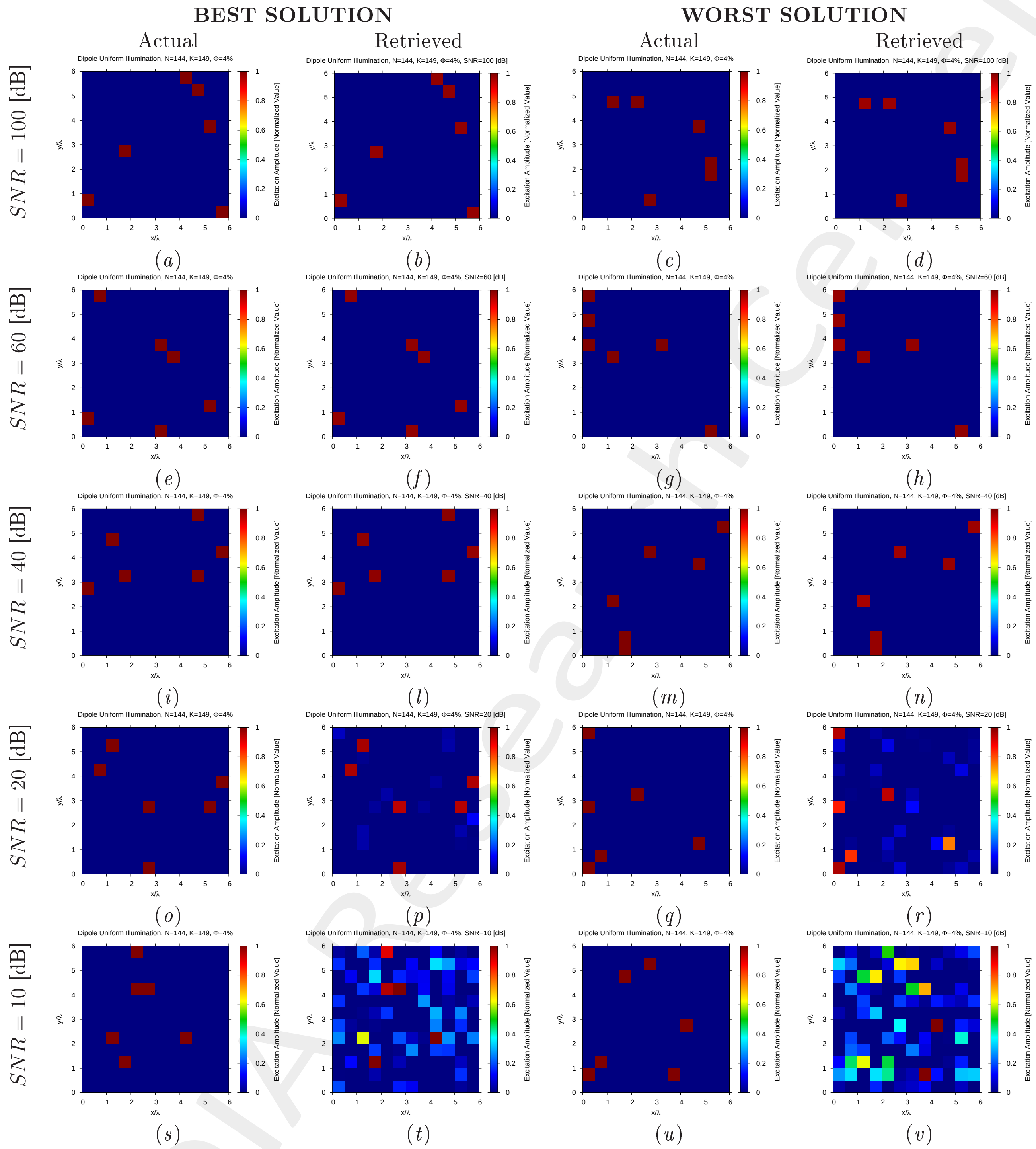


Figure 12: Uniform Dipoles Array ($N = 144$, $d_x = d_y = 0.5$ [$\lambda$], $\Phi = 4\%$) - Best and worst reconstructions by $BCS$ under several $SNR$ values.

### $\Phi = \frac{N_f}{N} = 8\%$ $(N_f = 12)$ - Best and Worst *BCS* Reconstructions

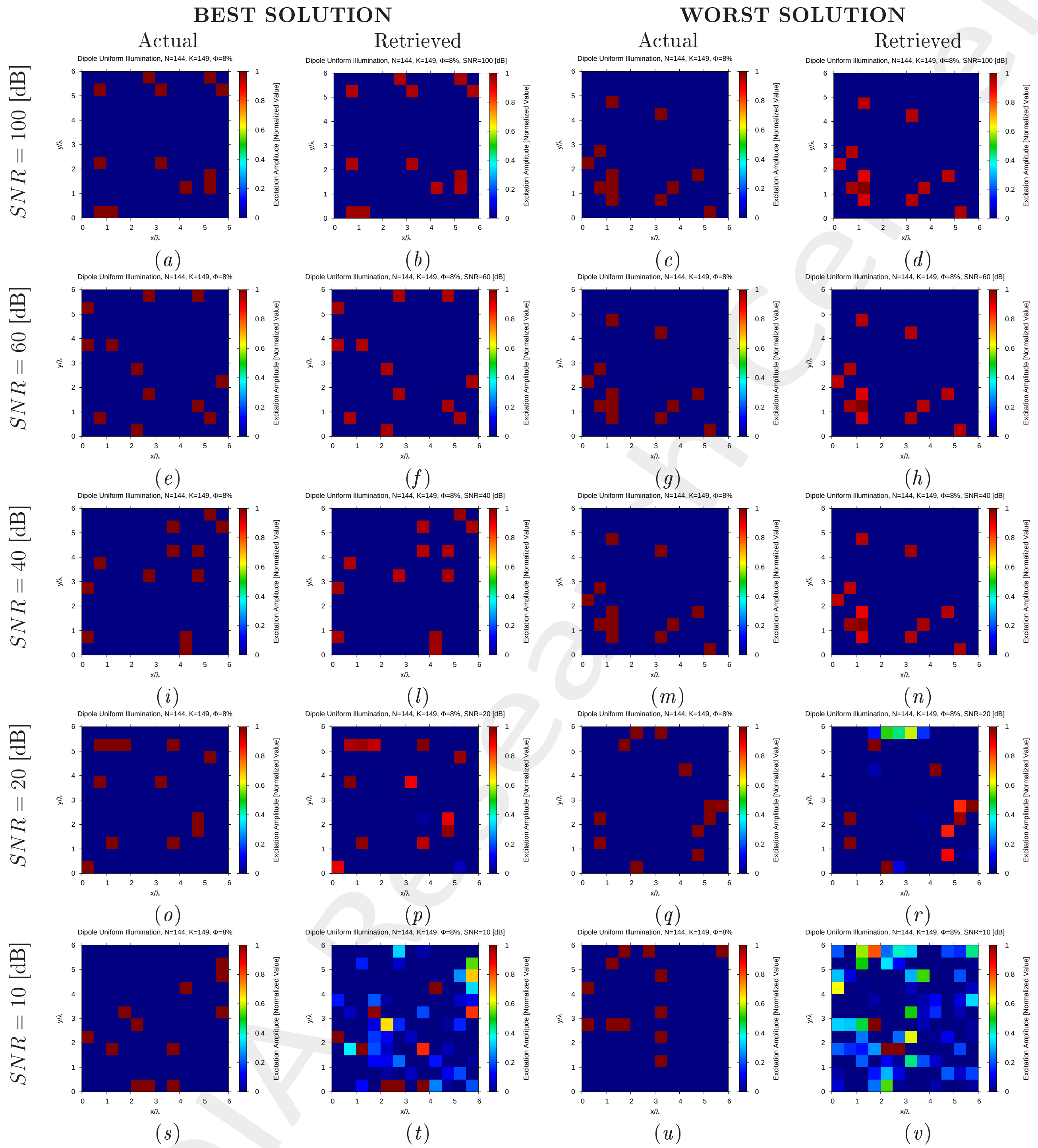


Figure 13: Uniform Dipoles Array ($N = 144$, $d_x = d_y = 0.5$ [$\lambda$], $\Phi = 8\%$) - Best and worst reconstructions by *BCS* under several *SNR* values.

$\Phi = \frac{N_f}{N} = 16\%$ ($N_f = 23$) - **Best and Worst** $BCS$ **Reconstructions**

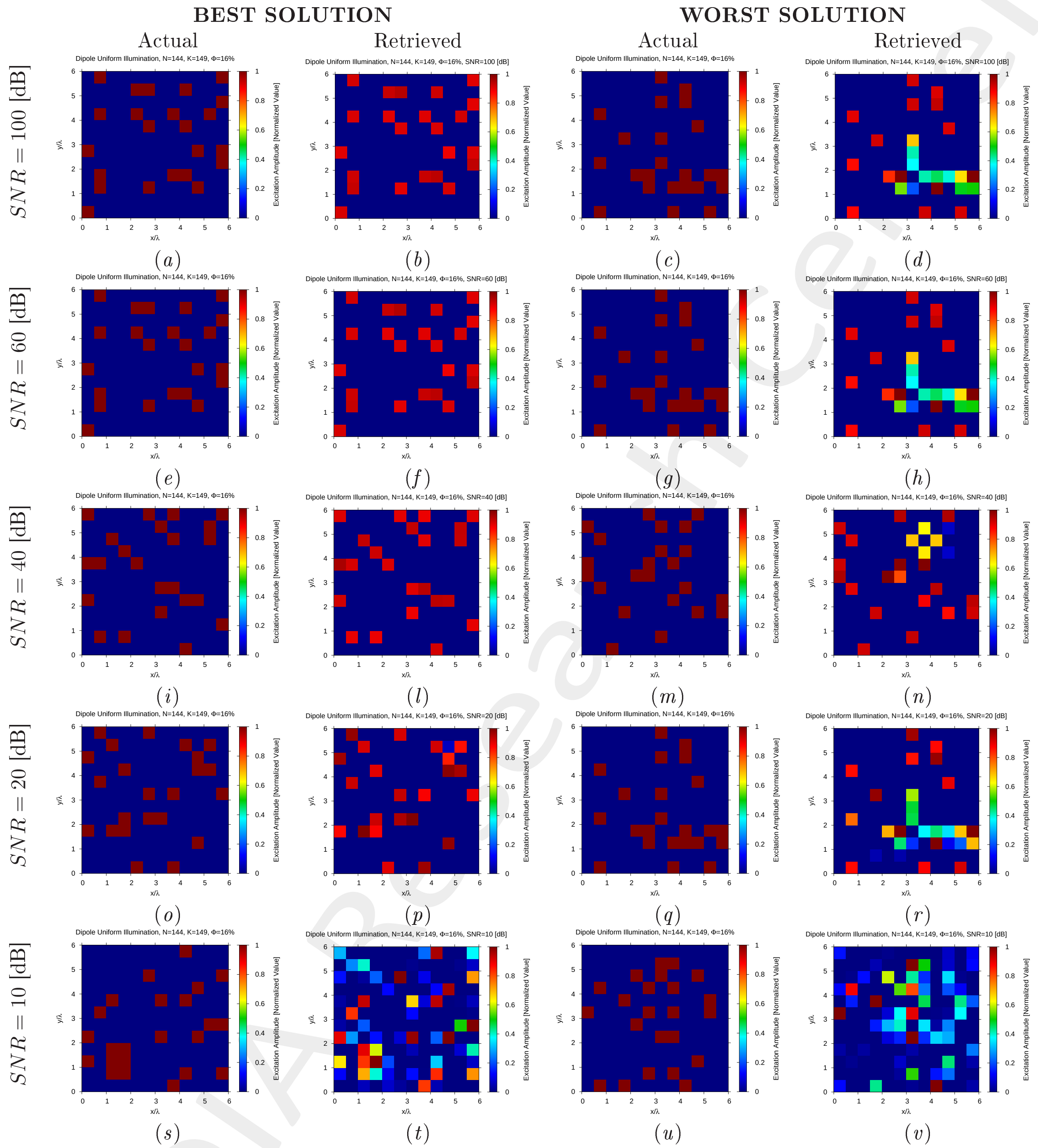


Figure 14: Uniform Dipoles Array ($N = 144$, $d_x = d_y = 0.5$ [$\lambda$], $\Phi = 16\%$) - Best and worst reconstructions by $BCS$ under several $SNR$ values.

## Diagnosis Error and Confidence Level

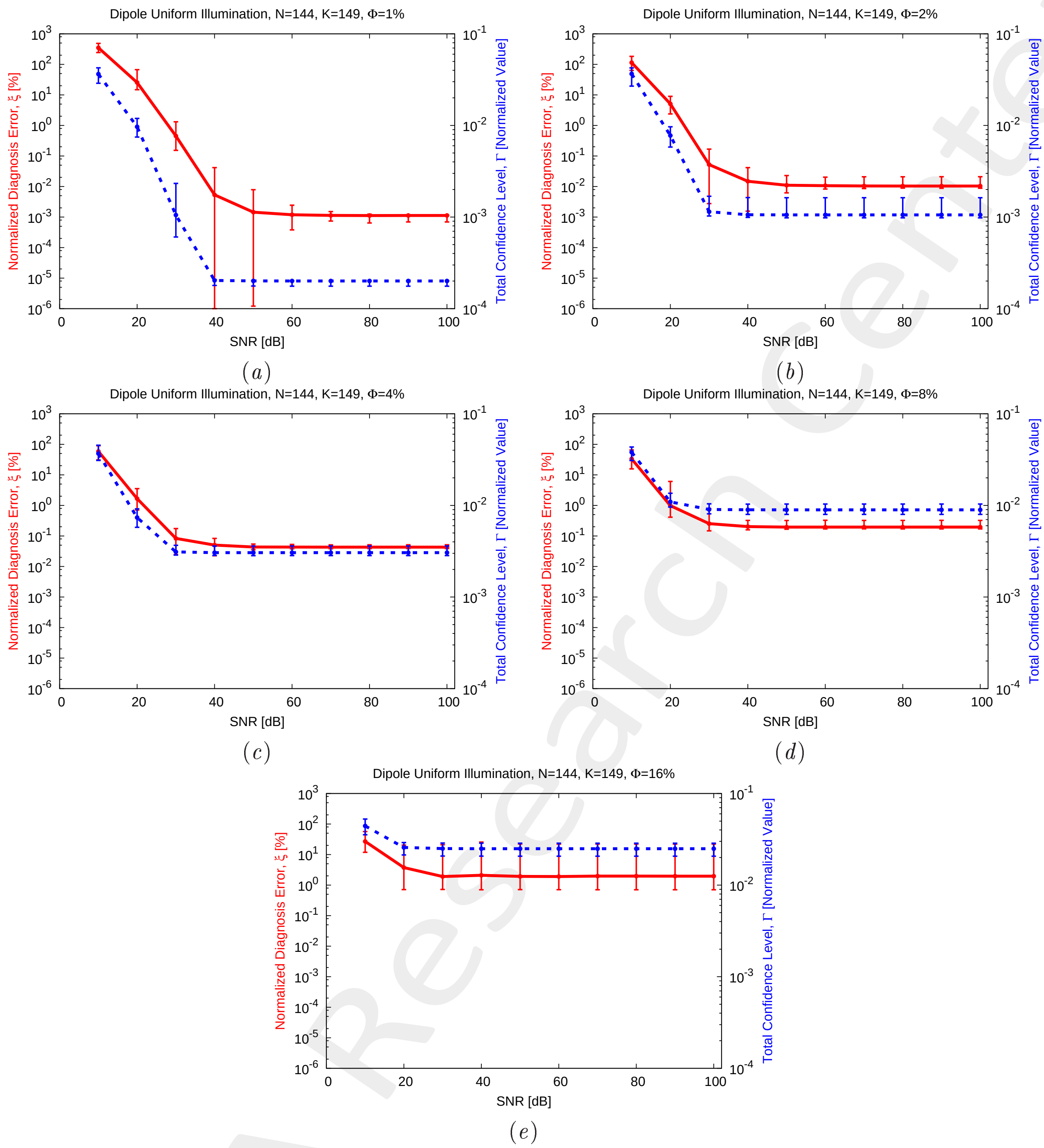


Figure 15: Uniform Dipoles Array ($N = 144$, $d_x = d_y = 0.5$ $[\lambda]$) - Behavior of the average, minimum and maximum diagnosis error ($\xi$) and total confidence level ($\Gamma$) versus the $SNR$, for $(a)$ $\Phi = 1\%$, $(b)$ $\Phi = 2\%$, $(c)$ $\Phi = 4\%$, $(d)$ $\Phi = 8\%$, and $(e)$ $\Phi = 16\%$.

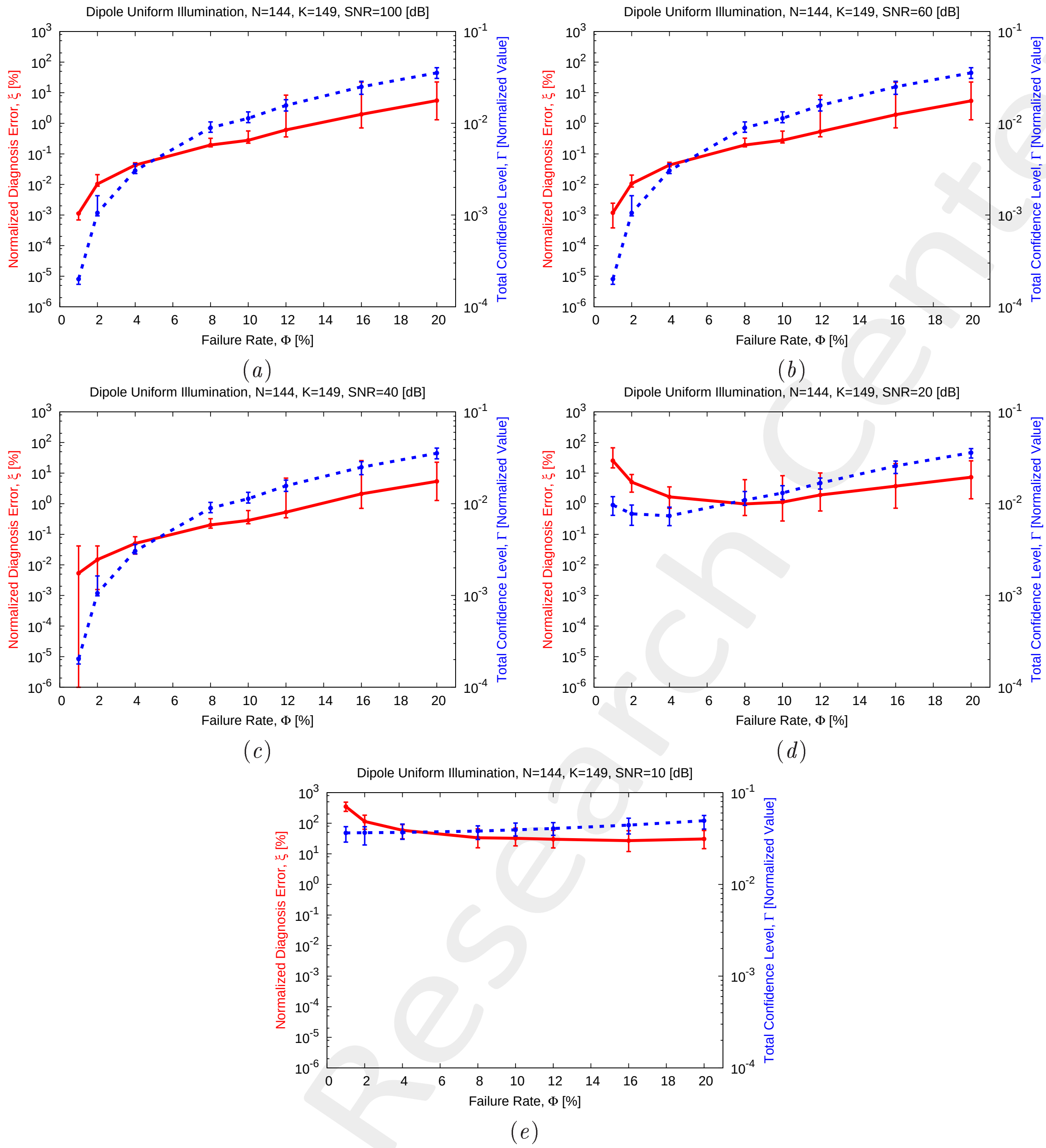


Figure 16: Uniform Dipoles Array ($N = 144$, $d_x = d_y = 0.5$ [$\lambda$]) - Behavior of the average, minimum and maximum diagnosis error ($\xi$) and total confidence level ($\Gamma$) versus the failure rate ($\Phi$), for ($a$) $SNR = 100$ [dB], ($b$) $SNR = 60$ [dB], ($c$) $SNR = 40$ [dB], and ($d$) $SNR = 20$ [dB].

## References


[1] P. Rocca, G. Oliveri, R. J. Mailloux, and A. Massa, "Unconventional phased array architectures and design methodologies - A Review," *Proc. IEEE*, vol. 104, no. 3, pp. 544-560, Mar. 2016.

[2] G. Oliveri, G. Gottardi, F. Robol, A. Polo, L. Poli, M. Salucci, M. Chuan, C. Massagrande, P. Vinetti, M. Mattivi, R. Lombardi, and A. Massa, "Co-design of unconventional array architectures and antenna elements for *5G* base stations," *IEEE Trans. Antennas Propag.*, vol. 65, no. 12, pp. 6752-6767, Dec. 2017.

[3] G. Oliveri, P. Rocca, and A. Massa, "Reliable diagnosis of large linear arrays - a Bayesian compressive sensing approach," *IEEE Trans. Antennas Propag.*, vol. 60, no. 10, pp. 4627-4636, Oct. 2012.

[4] M. Salucci, A. Gelmini, G. Oliveri, and A. Massa, "Planar arrays diagnosis by means of an advanced Bayesian compressive processing," *IEEE Trans. Antennas Propag.*, vol. 66, no. 11, pp. 5892-5906, Nov. 2018.

[5] A. Massa, P. Rocca, and G. Oliveri, "Compressive sensing in electromagnetics - A review," *IEEE Antennas Propag. Mag.*, pp. 224-238, vol. 57, no. 1, Feb. 2015.

[6] G. Oliveri, M. Salucci, N. Anselmi, and A. Massa, "Compressive sensing as applied to inverse problems for imaging: theory, applications, current trends, and open challenges," *IEEE Antennas Propag. Mag.,* vol. 59, no. 5, pp. 34-46, Oct. 2017.

[7] P. Rocca, M. A. Hannan, M. Salucci, and A. Massa, "Single-snapshot DoA estimation in array antennas with mutual coupling through a multi-scaling Bayesian compressive sensing strategy," *IEEE Trans. Antennas Propag.*, vol. 65, no. 6, pp. 3203-3213, Jun. 2017.

[8] M. Carlin, P. Rocca, G. Oliveri, F. Viani, and A. Massa, "Directions-of-arrival estimation through Bayesian Compressive Sensing strategies," *IEEE Trans. Antennas Propag.*, vol. 61, no. 7, pp. 3828-3838, Jul. 2013.

[9] L. Poli, G. Oliveri, P. Rocca, M. Salucci, and A. Massa, "Long-distance WPT unconventional arrays synthesis," *J. Electromagn. Waves Appl.*, vol. 31, no. 14, pp. 1399-1420, Jul. 2017.

[10] G. Oliveri, M. Salucci, and A. Massa, "Synthesis of modular contiguously clustered linear arrays through a sparseness-regularized solver," *IEEE Trans. Antennas Propag.*, vol. 64, no. 10, pp. 4277-4287, Oct. 2016.

[11] G. Oliveri and A. Massa, "Bayesian compressive sampling for pattern synthesis with maximally sparse non-uniform linear arrays," *IEEE Trans. Antennas Propag.*, vol. 59, no. 2, pp. 467-481, Feb. 2011.

[12] N. Anselmi, G. Oliveri, M. A. Hannan, M. Salucci, and A. Massa, "Color compressive sensing imaging of arbitrary-shaped scatterers," *IEEE Trans. Microw. Theory Techn.*, vol. 65, no. 6, pp. 1986-1999, Jun. 2017.

[13] N. Anselmi, G. Oliveri, M. Salucci, and A. Massa, "Wavelet-based compressive imaging of sparse targets," *IEEE Trans. Antennas Propag.*, vol. 63, no. 11, pp. 4889-4900, Nov. 2015.

[14] L. Poli, G. Oliveri, F. Viani, and A. Massa, "MT-BCS-based microwave imaging approach through minimum-norm current expansion," *IEEE Trans. Antennas Propag.*, vol. 61, no. 9, pp. 4722-4732, Sep. 2013.

[15] G. Oliveri, N. Anselmi, and A. Massa, "Compressive sensing imaging of non-sparse 2D scatterers by a total-variation approach within the Born approximation," *IEEE Trans. Antennas Propag.*, vol. 62, no. 10, pp. 5157-5170, Oct. 2014.

[16] L. Poli, G. Oliveri, and A. Massa, "Imaging sparse metallic cylinders through a local shape function bayesian compressive sensing approach," *J. Opt. Soc. Am. A*, vol. 30, no. 6, pp. 1261-1272, 2013.

[17] L. Poli, G. Oliveri, P. Rocca, and A. Massa, "Bayesian compressive sensing approaches for the reconstruction of two-dimensional sparse scatterers under TE illumination," *IEEE Trans. Geosci. Remote Sens.*, vol. 51, no. 5, pp. 2920-2936, May 2013.

[18] L. Poli, G. Oliveri, and A. Massa, "Microwave imaging within the first-order Born approximation by means of the contrast-field Bayesian compressive sensing," *IEEE Trans. Antennas Propag.*, vol. 60, no. 6, pp. 2865-2879, Jun. 2012.

[19] G. Oliveri, L. Poli, P. Rocca, and A. Massa, "Bayesian compressive optical imaging within the Rytov approximation," *Opt. Lett.*, vol. 37, no. 10, pp. 1760-1762, 2012.

[20] G. Oliveri, P. Rocca, and A. Massa, "A Bayesian compressive sampling-based inversion for imaging sparse scatterers," *IEEE Trans. Geosci. Remote Sens.*, vol. 49, no. 10, pp. 3993-4006, Oct. 2011.

[21] N. Anselmi, L. Poli, G. Oliveri, and A. Massa, "Iterative multi-resolution bayesian CS for microwave imaging," *IEEE Trans. Antennas Propag.*, vol. 66, no. 7, pp. 3665-3677, Jul. 2018.

[22] L. Poli, P. Rocca, G. Oliveri, and A. Massa, "Failure correction in time-modulated linear arrays," *IET Radar, Sonar & Navigation*, vol. 8, no. 3, pp. 195-201, 2014.